Acta Mechanica 73, 77–93 (1988)

ACTA MECHANICA

An Experimental Investigation of the Reynolds Number Effect on a Normal Shock Wave-Turbulent Boundary Layer Interaction on a Curved Wall[1]

By

P. Doerffer, Gdańsk, Poland, and **J. Zierep**, Karlsruhe, Federal Republic of Germany

With 11 Figures

(*Received August 24, 1987*)

Summary

The presented experiment concerned an interaction between a normal shock wave, terminating a local supersonic area in a curved duct, and a turbulent boundary layer developed along the convex wall. This paper deals with the Reynolds number effect upon the interaction structure.

The measurements included flow parameters distribution determination, boundary layer development through the interaction area and the shock wave topography visualization. In order to gain more information about separation the wall oil tracing has been applied. The comparison of our results with other published data is presented.

1. Introduction

Modern commercial airplanes cruise with speeds that exceed the "critical" speed. This means limited supersonic regions development on the upper side of the wings. The supersonic area is terminated downstream by a normal shock wave that interferes with the wall boundary layer. It distorts the usually turbulent boundary layer.

This region is of great interest and concern to airplane designers as it is a source of drag, loss of lift, separation of the boundary layer and buffeting (oscillations of the shock wave causing serious oscillations of wings).

One of the first publications, dealing with the influence of the shock wave downstream of a supersonic region on a convex wall, is due to Ackeret et al. [1]. They have investigated the boundary layer determination at the interaction region and found that the observed effects are a function of the free stream

[1] The experiments have been carried out at the Institut für Strömungslehre und Strömungsmaschinen, Karlsruhe Universität, Karlsruhe, Federal Republic of Germany.

Mach number upstream the shock wave. The characteristic Reynolds number for the interaction process is based on the undisturbed boundary layer thickness and the flow parameters at its outer edge.

2. Theoretical Considerations

The actual interest of airplane designers in the problem of shock wave-boundary layer interaction on the convex upper side of wings has accelerated the investigation of this flow field region. Two ways of approach are in use:

(i) matching of the inviscid external flow field with the inner viscous layer, which are calculated independently

(ii) the numerical solution of the complete Navier-Stokes equations.

The first method is successful for not separating flows up to the incipient separation. The computer time used for this method of matching is relatively small [20], [21].

The experiments of Ackeret et al. [1] showed for the first time that immediately downstream the shock wave an afterexpansion can be observed. Oswatitsch and Zierep [23] confirmed theoretically an existance of the afterexpansion for an inviscid flow. The convex wall causes a logarithmic singularity at the shock that leads to the observed afterexpansion. For treating the viscous case, Bohning and Zierep [20] splitted the interaction region into three layers:

(i) an outer inviscid transonic flow with a singularity (transonic nonlinear potential equation).

(ii) a boundary layer outer region with compressibility and friction, introduced by means of the velocity profile,

(iii) and a lowest layer at the wall with full friction effects (Navier Stokes equation).

The analysis has been done quantitatively for a number of conditions concerning the Mach number, Reynolds number and wall curvature up to the incipient separation. The increase of the Mach number rises the tendency of the flow to a shock induced separation. This model has been treated numerically by Koren and Bannink [21]. The numerical solution allows a large variety of the boundary layer flow parameters.

Another theoretical approach to the normal shock wave-turbulent boundary layer interaction employs full Navier-Stokes equations. This is presented in [14], [16], [18], [22], [24]. Computer codes employing the Navier-Stokes equations are attractive because they compute simultaneously viscous and inviscid flow fields.

The used equations are time-dependent, mass-averaged for compressible flow. They are augmented by the equations associated with used turbulence model.

The obtained results are quite good for nonseparating interactions but are rather poor when separation occures. In the last case an applied turbulence model has a significant effect on the obtained results.

Developed computer codes provide a good tool for the interaction behaviour analysis. Good quantitative results have been obtained for some particular cases.

3. Experiment

A lot of research work has been already carried out dealing with detailed distribution of the flow parameters, shock bifurcation topography, separation development and turbulence properties behaviour in the interaction area. Quite often they were performed in order to provide experimental information for verification of theoretical results.

In most of the reported experimental investigations shock waves were generated on flat walls [2], [3], [4], [5], [6], [8]. Considered interaction however, takes place usually on curved surfaces of airfoils, turbine blades and transonic intakes. Therefore our investigation is carried out on a curved wall with a boundary layer thickness-wall curvature ratio at a magnitude corresponding to technical applications. A literature representation of curved wall cases is very limited and includes the experiments of Ackeret et al. [1] of 1946, Bohning and Zierep [20], Nebbeling [10] and some of Delery's experiments [7] should also be added up to this group.

Our experimental arrangement has been set up so, that it allows to investigate a turbulent boundary layer normal shock wave interaction on a convex wall with a possibility for a separate control of the Mach and the Reynolds number [9], [11], [12], [17].

The developed facility allows to investigate the interaction at a certain range of Reynolds number $\mathrm{Re}_{\delta u}$ and Mach number M.

The presented paper deals with the $\mathrm{Re}_{\delta u}$ effect on the interaction structure for a relatively high Mach number, e.g. with a well developed λ-foot. The literature data concerning the influence of $\mathrm{Re}_{\delta u}$ at constant M value are more reliable as it is much easier to keep M constant. Therefore this was our first step. It should be emphasized however that the available published data that could be used for comparison are very limited and therefore the flat wall flow results are also refered to. Available, published curved wall flow measurements concern only single combinations of $\mathrm{Re}_{\delta u}$ and M.

The experimental investigation has been carried out in the transonic wind tunnel at the Institut für Strömungslehre und Strömungsmaschinen of the Karlsruhe University [9]. It is a short duration, suction type wind tunnel.

The test section is presented in Fig. 1.

The desired flow field is obtained in a curved duct which is 50 mm wide and about 150 mm high. The local supersonic area is formed at the convex wall

and is terminated by a normal shock wave that interacts with a turbulent boundary layer, developed on the convex wall.

The stagnation parameters in our wind tunnel are equal to the ambient conditions. This eliminates these parameters as means of Reynolds number control. The characteristic Reynolds number for the interaction is based on the undisturbed boundary layer thickness δ_u. This imposes the δ_u control as the only means of the $\mathrm{Re}_{\delta u}$ variation. Several methods of δ_u change have been tested [9], and the one selected for application is presented in Fig. 1. This is a step-slot arrangement. It allows to control the boundary layer thickness by a variable step height and by an additional stream bleeding through the slot.

This paper concerns an investigation of a Reynolds number effect on the interaction at the highest Mach number, obtainable in our test facility, it is $M_w = 1.47$. M_w is a maximum wall Mach number value calculated from the wall static pressure and the stagnation pressure upstream of the interaction. It should be realised that this Mach number value does not exist in the flow field. In the curved duct M decreases with an increasing distance from the convex wall. The duct curvature causes a static pressure gradient across the channel, including the boundary layer. Regarding this, the Mach number at the boundary layer is a little smaller than the ideal Mach number at the wall M_w. In the same flow field the Mach number at the boundary layer edge is dependent on the boundary layer thickness δ. In order to investigate the Re effect, the flow field must be the same for all cases. To secure this the wall Mach number must be held constant over the whole investigation.

The Reynolds number range is limited by the possible boundary layer thickness variation. Four cases of δ_u have been included. These are $\delta_u = 3.2$; 5.6; 7.6; 9.1 mm, what corresponds to $\mathrm{Re}_{\delta u} = 5.5$; 9.7; 13.1; $15.3 \cdot 10^4$ respectively.

For data reduction details the reader is refered to [17].

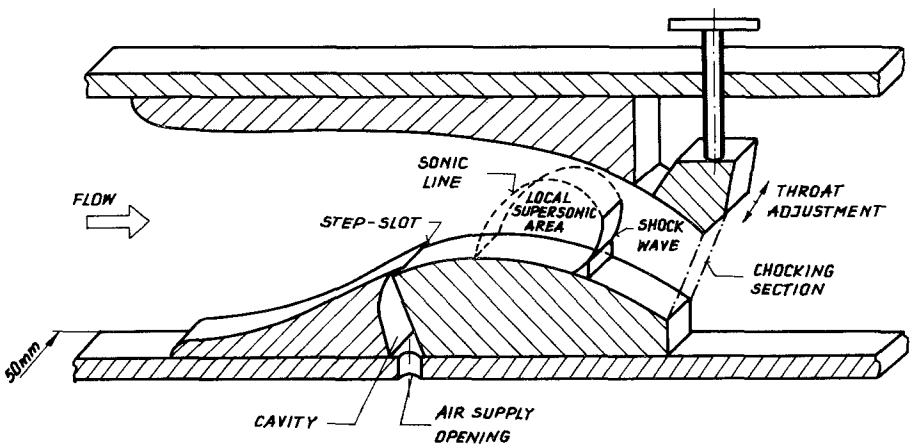

Fig. 1. Test section arrangement

The wall static pressure distribution obtained from the four cases are assembled in Fig. 2. For the comparison purposes normalized coordinates are used. The static pressure is normalized with a minimum value of its distribution. The distance along the wall is normalized with an undisturbed boundary layer thickness. These distributions are set up together so that the point $x/\delta_u = 0$ denotes the bifurcation point location. Thanks to this, it is indicated how far upstream of the main shock the pressure disturbance reaches along the wall. It has been noticed that the disturbance penetrates much further upstream for lower $\mathrm{Re}_{\delta u}$ values. In accordance with this observation is the difference in the slope of a steep static pressure rise.

It has been noticed by Seddon [2] that this rise is at the beginning linear up to the "kink point" where the decrease of the pressure gradient starts. The level of the kink pressure $(P_s/P_0)_k$ increases with the $\mathrm{Re}_{\delta u}$ value increase. This tendency is also reported in [4].

The maximum slope of the static pressure distribution increases for the increasing $\mathrm{Re}_{\delta u}$, what is in agreement with [4], [16], [18]. The distance between the beginning of an interaction and the "kink point" is called by Seddon a "shock phase". The length of this phase normalized with δ_u decreases considerably with the increasing $\mathrm{Re}_{\delta u}$ in agreement with [4].

An example of a Schlieren picture of an investigated *flow topography* is presented in Fig. 3. The flow direction on this picture is from left to right. The

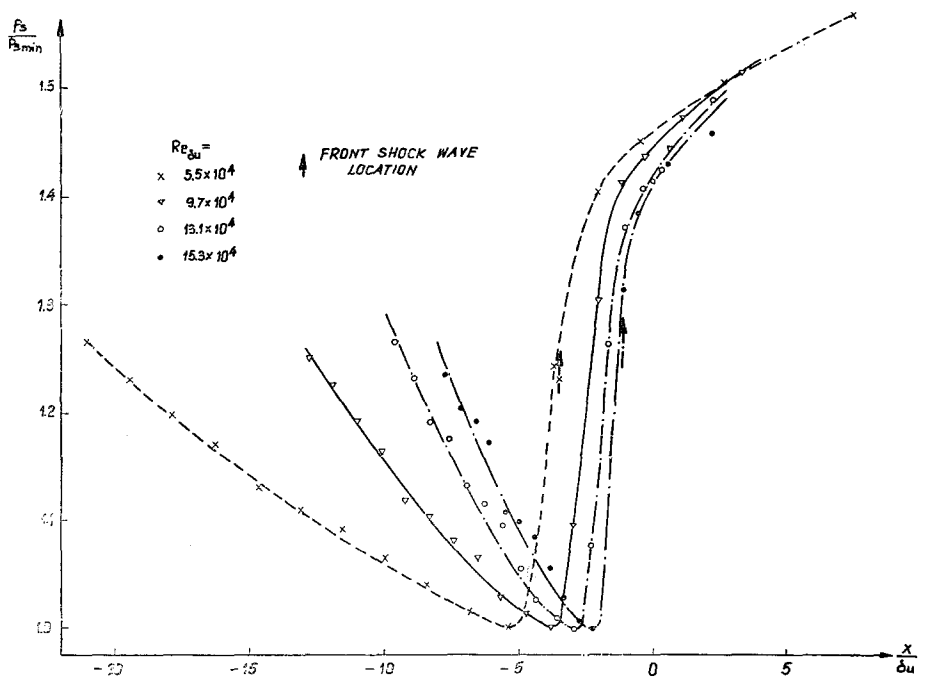

Fig. 2. Wall static pressure distribution

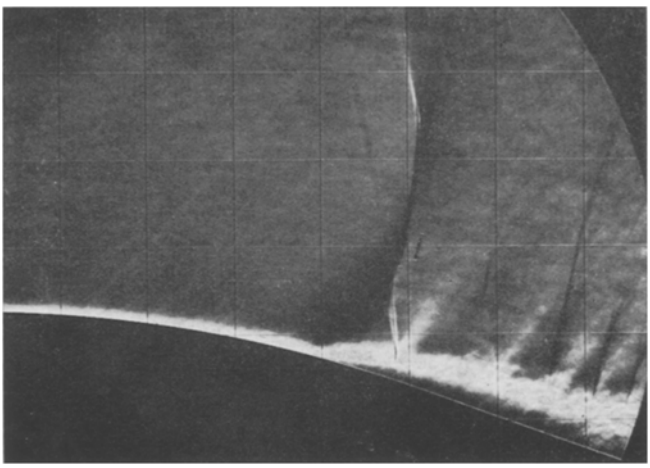

Fig. 3. Schlieren picture of the flow $M = 1.47$; $\mathrm{Re}_{\delta u} = 5.5 \cdot 10^4$

most important detail is the shock wave. Starting from the upper rim of the photograph the transition of the sonic line to the normal shock is observed. The normal shock (called here the main shock) is curved a little and comes down to the bifurcation point, forming a λ-foot. Downstream the bifurcation point one can observe a shade of the vortex sheet. This is due to the different total pressure drop in a normal shock and in the shock sequence. The first pressure disturbance at the wall forms a compression wave originating within the boundary layer, which builds up the front shock wave. This shock begins to have a noticable intensity in a distance from the wall. At the bifurcation point it is still embeded in a compression wave.

The rear shock, below the bifurcation point bends downstream and then remains straight until the boundary layer is reached. This shock penetrates the boundary layer where it bends again to become normal to the wall. The rear shock is "*s*" shaped.

The white zone along the convex wall indicates the boundary layer. The edge of the white zone could be roughly interpreted as the boundary layer edge. The compression at the λ-foot front branch has a very strong effect on the boundary layer. A very strong thickness increase takes place until the rear shock weakens this process. Large turbulent structures are generated. The boundary layer thickness increases still downstream of the shock but not as much as between the λ-foot shocks.

One of the most important outputs from presented type of investigation is the *flow parameter distribution* in the interaction area.

An example of the flow topography, based on iso-Mach number lines is presented in Fig. 4. These iso-Mach lines are constructed on nine or eight measurement traverses, whose locations are marked in the picture. In all cases the shock topography is very similar. Upstream of the interaction the iso-Mach lines are

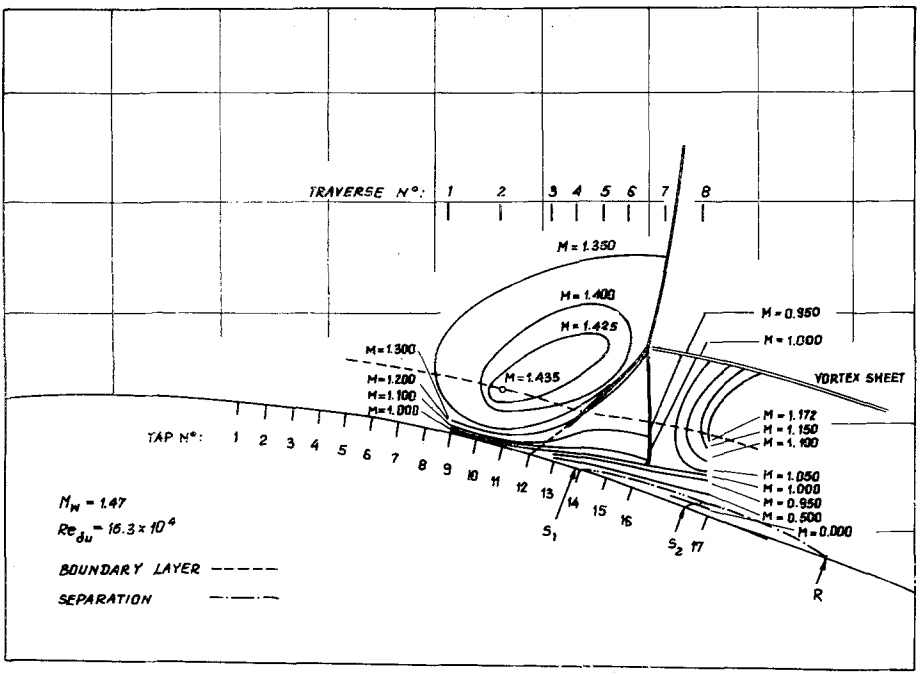

Fig. 4. Flow topography, iso-Mach lines

closed. The reason for this is that upstream of the shock wave the Mach number increases towards the shock and towards the convex wall. On the other side in the vicinity of the λ-foot front shock M decreases towards the shock and within the boundary layer M decreases towards the wall. This results in a Mach number maximum build up which lies at the boundary layer edge and is located upstream of the front shock due to the existance of the compression zone. This location is confirmed by the wall static pressure distribution. The beginning of the wall static pressure deviation from the upstream gradient takes place at the flow field maximum Mach number streamwise location.

The flow between the two λ-foot shocks and the edge of the boundary layer looks the same in all cases but differs in size. The area displays nearly constant Mach number. Due to this the rear shock is mostly straight. A weak curvature of the rear shock under the bifurcation point reflects the Mach number gradient at the front shock. Then the rear shock is straight as the Mach number is nearly constant above the boundary layer. This Mach number value is the same for all cases. Then within the boundary layer the rear shock bends again, becoming normal to the wall and disappears deep within the boundary layer at the $M = 1.0$ line. Between λ-foot branches the boundary layer thickness increases considerably, and for the thinner boundary layer this increase is much more pronounced.

Just downstream of the rear shock the flow is subsonic with increasing Mach numbers towards the wall. Upstream the rear shock within the boundary layer

M becomes lower, the shock weaker and M after the shock higher. In all cases an after-expansion with supersonic velocities has been detected. The sonic line originates from the area of the rear shock disappearance in the boundary layer. The iso-Mach lines go very steep upwards. It looks that the expansion is concentrated within the boundary layer just downstream of the rear shock. This is confirmed by a white zone present at this place in the Schlieren picture (Fig. 3).

The shape of the observed supersonic part of the after expansion is in agreement with the shape reported by other authors in [3], [8], [10], [14]. Therefore our measurements do not support Seddon's supersonic tongue shape [2] and the subsonic after expansion of Padova and Falk [4].

The interaction *effect on the boundary layer* should be discussed on the distribution of the boundary layer and displacement thickness (δ, δ_1) and the shape factor based on δ_1 and momentum thickness. Boundary layer thickness distribution for two extreme $\mathrm{Re}_{\delta u}$ values are presented in Fig. 5a. All distances have been normalized with an undisturbed boundary layer thickness. Positions of the front and rear shock at the boundary layer edge are marked at the distribution curves. $x/\delta_u = 0$ refers to the main shock locations and to the wall static pressure presentation (Fig. 2). The evident kinks of the δ distribution appear at the shock locations. It is difficult to say if this is a shock effect on the boundary layer thickness or on the measurement error. The rate of the boundary layer thickness increase is the same in this coordinate system, but its magnitude is much larger for a smaller $\mathrm{Re}_{\delta u}$. Unfortunately, the here presented measurement does not include the boundary layer rehabilitation phase. At our last traverse the boundary layer thickness still increases significantly for $\mathrm{Re}_{\delta u} = 5.5 \cdot 10^4$ and starts to decrease its gradient for $\mathrm{Re}_{\delta u} = 15.3 \cdot 10^4$. Schlieren pictures indicate that at this area the rates of the boundary layer thickness increase should start to drop down.

A similar behaviour is performed by the displacement thickness distribution (Fig. 5b). The δ_1 is normalized with δ_u. The distribution curves have a very small point scatter. At the beginning the curves are horizontal. Then in the area of λ-foot front location the displacement thickness starts to increase with a constant gradient within the whole remaining part of a measurement zone. This gradient seems to be independent of $\mathrm{Re}_{\delta u}$.

The measurements have not been continued into the rehabilitation phase, therefore no decrease of the gradient is observed. The magnitude of the displacement thickness increase is much higher for smaller $\mathrm{Re}_{\delta u}$.

Fig. 5c presents the shape factor distribution. It is often accepted that separation takes place at a shape factor 2.6. This value has been marked in the presented diagram.

The comparison of the boundary layer parameters (δ, δ_1) indicate without any doubt that at a higher $\mathrm{Re}_{\delta u}$ the interaction effect on the boundary layer is smaller.

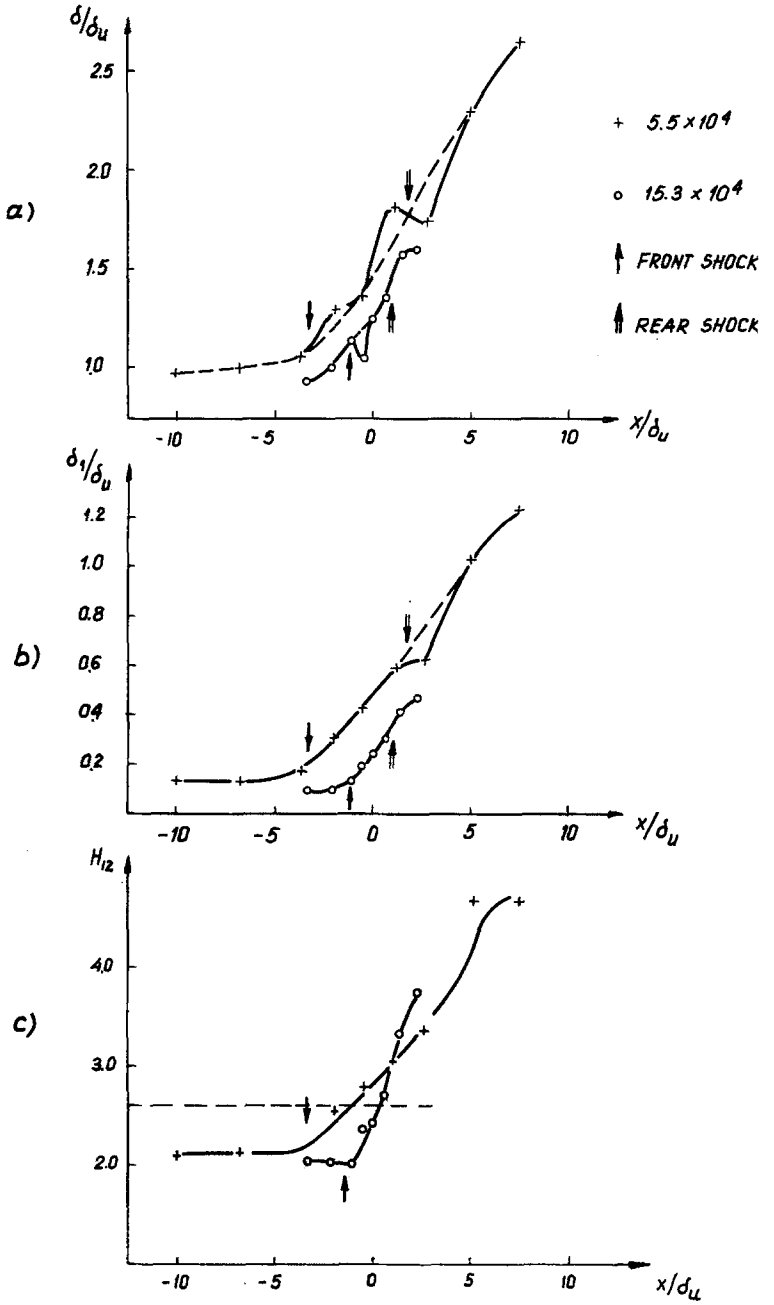

Fig. 5. Boundary layer parameters

a) Boundary layer thickness; b) Displacement thickness; c) Shape factor

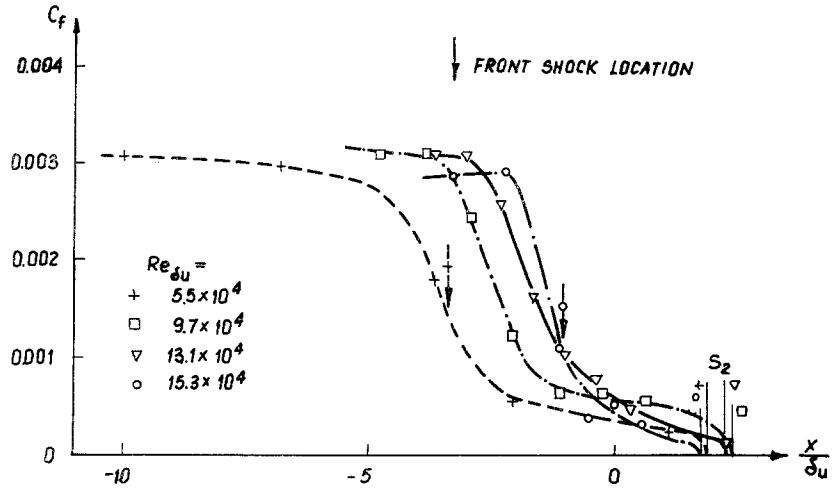

Fig. 6. Skin friction distribution

The last information extracted from the boundary layer profiles measurement is the *skin friction coefficient* (c_f) distribution. It has been obtained from the fit to the law of the wall. The assembly of the c_f distribution for all cases is presented in Fig. 6. The distance along the wall is normalized with δ_u and $x/\delta_u = 0$ refers to the main shock location again.

The skin friction coefficient value of the undisturbed profiles is for all $\mathrm{Re}_{\delta u}$ cases about the same $c_f \geqq 0.003$.

Under the λ-foot front shock the c_f value drops down rapidly. For the limiting cases the front shock location is marked at the distribution curves. It is observed that the c_f drop starts upstream of the front shock position. The sudden increase of the wall static pressure is connected with a sudden decrease of the c_f value.

Our measurements show an untypical c_f behaviour at separation. The regular c_f distribution, as observed by other authors, should continue to drop below the $c_f = 0$, reach a minimum value and then rise to reach positive values through the reattachement point. In our measurements the sharp c_f drop is not continued to negative values. At very low c_f values the distribution curves level off. Then a slow decrease takes place and separated profiles are reached further downstream. The c_f distributions would mean that the separation takes place downstream of the shock system. It is however expected that the separation takes place just downstream the area where the λ-foot front shock interacts with the boundary layer. This idea would be supported by the δ and δ_1 behaviour in our measurements and by the first strong c_f drop.

The other authors find a separation point in this location too. If the sharp c_f drop is extrapolated to $c_f = 0$, the obtained location would coincide very well with an expected place. Such a location is marked with s_1 in Fig. 4.

In order to clarify this strange c_f behaviour a wall friction lines pattern

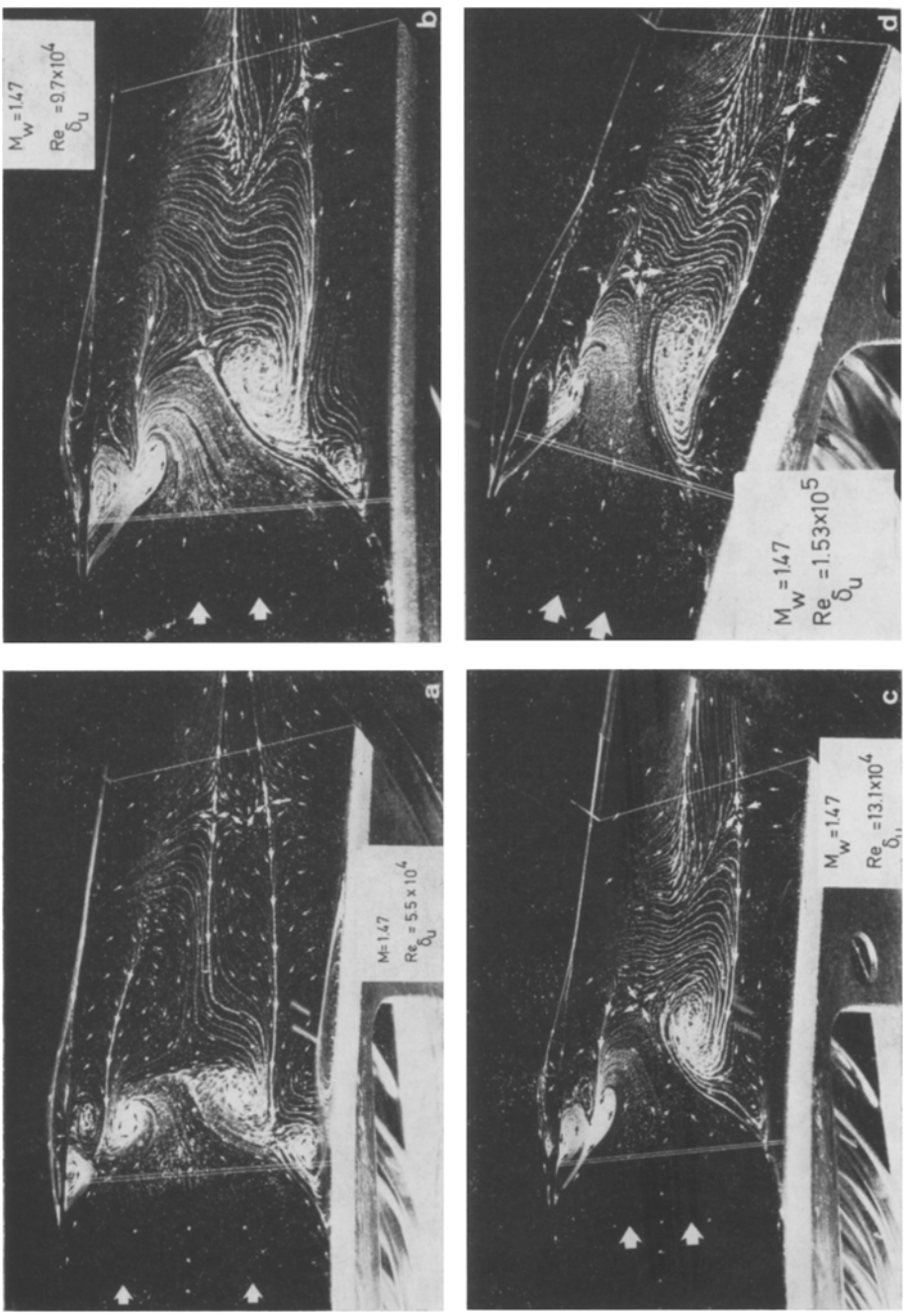

Fig. 7. Oil visualization

a) $\mathrm{Re}_{\delta u} = 5.5 \cdot 10^4$; b) $\mathrm{Re}_{\delta u} = 9.7 \cdot 10^4$; c) $\mathrm{Re}_{\delta u} = 13.1 \cdot 10^4$; d) $\mathrm{Re}_{\delta u} = 15.3 \cdot 10^4$

has been investigated by means of the *oil visualization* method. The wall skin friction lines patterns for all investigated cases are presented in Fig. 7. These present a view of the convex wall through the tunnel window. Two large arrows on the left hand side of the picture indicate the flow direction. Small arrows alligned with the oil streaks show the wall flow direction and middle size arrows mark the critical points and separatrices.

The double line, drawn across the convex wall, indicates the λ-foot front shock position. The single line is drawn for reference only and indicates an edge of the tunnel windows.

The detailed discussion of the separation structure is presented in a separate paper [19]. As it is observed in Fig. 7 the $\mathrm{Re}_{\delta u}$ has no effect on the pattern itself but the $\mathrm{Re}_{\delta u}$ increase magnifies the asymmetry of the pattern. In order to make the discussion of the pattern more easy a sketch of the most important details is presented in Fig. 8. This sketch concerns an example of $\mathrm{Re}_{\delta u} = 15.3 \cdot 10^4$.

The disturbance of the wall flow starts upstream of the front shock location in the convex-side walls corner. This place coincides with the wall static pressure minimum location (between taps 10 and 11). From this place starts a strong wall stream contraction. At the front shock location δ and δ_1 begin a significant increase and c_f drops very sharp. On movie film one can observe a very significant decrease of the oil flow velocity, which corresponds to the c_f drop. With this slow motion oil follows the contraction downstream the shock position. Then it splits up, forms a saddle point of separation S_A and turns sideways into the focuses V_R (right) and V_L (left). The lack of the reverse flow in the middle of the channel just downstream the front shock, the downstream shift of the S_A confirm the correctness of c_f behaviour, infered from the velocity profiles. The saddle location

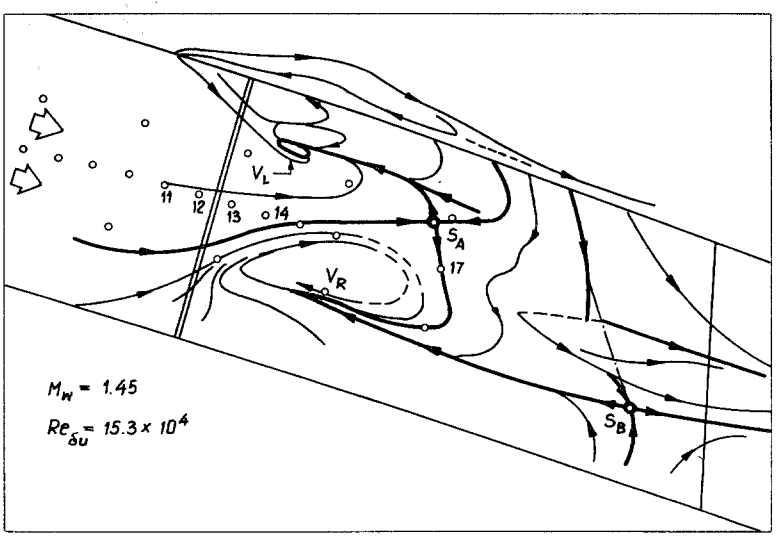

Fig. 8. Skin friction lines pattern $\mathrm{Re}_{\delta u} = 15.3 \cdot 10^4$

S_A is plotted in Fig. 6 and marked as S_2. This provides the $c_f = 0$ point for the presented distributions. S_2 is also marked in Fig. 4. It is very strange that the S_2 location is far downstream of the expected place S_1, where δ and δ_1 distributions and also the significant c_f drop would infer separation. At S_2 location the pressure jump at the wall is completed and only small adverse gradient remains, the displacement thickness is five times greater than in undisturbed flow area.

The problem of 3-D effects in the separation area is presented in [19]. The topological structures of separation and asymmetry of these structures is discussed there.

In spite of all reasons presented in [19], the *separation length* has been defined as a distance between S_1 and reattachment. It has been done only for comparison purposes. Its comparison with measurements of another author is presented in Fig. 9. Our experimental points and one of Nebbeling are the only results of flows over a curved wall. The maximum Mach number at the edge of the boundary layer is $M \approx 1.435$ which is almost the same as in the case of Nebbeling ($M = 1.43$).

The $\mathrm{Re}_{\delta u}$ values in our investigations are a little lower than most of the compared results. The shape of our curve is steeper than that of others for flat

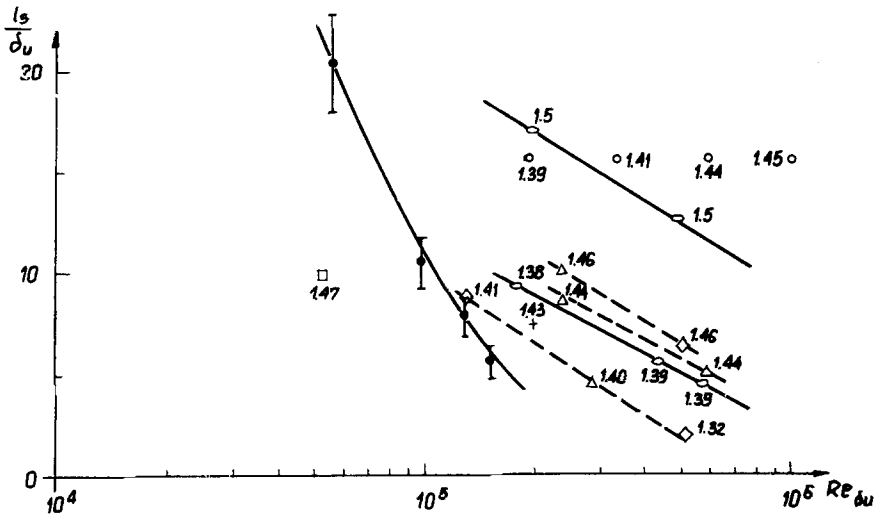

SYMBOL	REF.	METHOD
△	KOOI	LAW OF THE WALL
□	SEDDON	" " " "
⬭	EAST	" " " "
△	MATEER	" " " "
○	"	HOT WIRES IN SURFACE
◇	VIDAL	C_f (TRANSDUCER)
+	NEBBELING	WALL LAW + PRESTON TUBE
•	PRESENT RESULT	WALL LAW + OIL VIS.

NUMBER AT SYMBOLS INDICATE MACH NUMBER

Fig. 9. Separation length

wall flow. However the other slops are based on two point characteristics, what is not very reliable. The difference in the gradient could mean that l_s is more sensitive to the Reynolds number in the case of curved wall. To help the interpretation of our curve the points are fitted with error bands. Taking into acount our point for the highest $\mathrm{Re}_{\delta u}$, Nebbeling's point and the lowest $\mathrm{Re}_{\delta u}$ case of Kooi one could try to draw conclusions about the wall curvature effect on the separation. Kooi's experiment has been carried out on a flat wall. Nebbeling used a curved wall with $R = 500$ mm and we had a wall with $R = 300$ mm. It could then be noticed that the separation length decreases with increasing curvature. That is, the favourable pressure gradient in an undisturbed flow counteracts the development of the separation.

The last experimental result to be discussed here is the *shock wave bifurcation topography*. Two dimensions are considered:

— bifurcation point height "h" measured normal to the wall,
— distance "l" between the front and rear shocks at the wall.

The wall location of the rear shock is easy to determine as near the wall the shock is normal. The location of the front shock position is not as straightforward, the shock wave has been extrapolated down to the wall to obtain a shock wall position.

The bifurcation point height comparison with available literature data is presented in Fig. 10. In the available publications the data consist of single points and only Calspan's results provide a two point characteristic. Our curve is

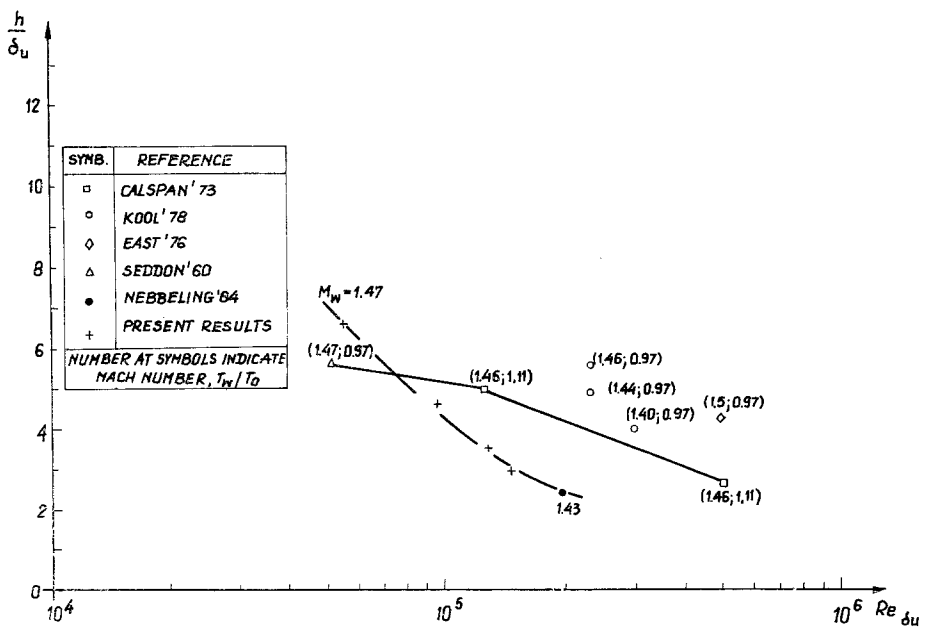

Fig. 10. Bifurcation point height

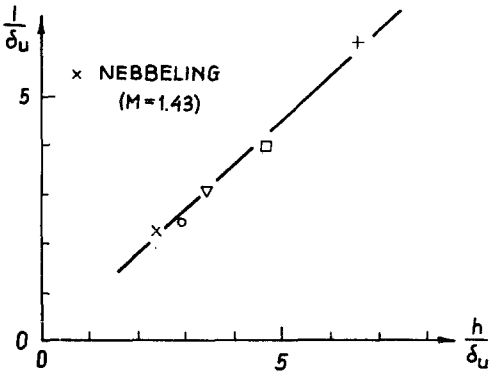

Fig. 11. λ-foot topography

the only one based on more than two points. At higher $\mathrm{Re}_{\delta u}$ our measurements indicate smaller values then the flat wall results of other authors. The only curved wall result obtained from literature (Nebbeling) fits very well into the extrapolation of our characteristic. A $\mathrm{Re}_{\delta u}$ increase causes the normalized bifurcation height to decrease substantially.

An additional information is provided by the Fig. 11. It presents a relation between bifurcation point height and a wall distance between shocks. The characteristic is linear and inclined by nearly 45°. The point of Nebbeling fits to our curve very well. This means that the shock bifurcation topography displays similarity when changing its size with $\mathrm{Re}_{\delta u}$. This conclusion contradicts the Padova and Falk [4] observation, who have found a significant change in an angle formed by the bifurcation shock branches.

4. Conclusions

The results of carried out measurements allow to state the below listed conclusions.

(i) At $M_w = 1.47$ and $5.5 \cdot 10^4 \leqq \mathrm{Re}_{\delta u} \leqq 15.3 \cdot 10^4$ the shock bifurcates and a large λ-foot is developed. Its interaction with a turbulent boundary layer cause the flow separation.

(ii) Pressure jump at the wall takes place much further upstream the main shock location for lower $\mathrm{Re}_{\delta u}$ values, and simultaneously the kink pressure level, the maximum slope of pressure jump decreases and the shock phase length increases.

(iii) The first pressure disturbance at the wall generates a compression wave that develops a shock wave. It is quite strong at the bifurcation point but still embedded within the compression wave.

(iv) Rear shock is "S" shaped and penetrates the supersonic part of the boundary layer. It is followed by the after expansion, which is centered within the boundary layer.

(v) The after expansion accelerates the flow to supersonic velocities once again. Its shape contradicts the Seddon result [2] and a subsonic after expansion found by Padova and Falk [4]. It is in agreement with the results published in [3], [8], [10], [14].

(vi) At the λ-foot front branch location at the wall the static pressure has completed over a half of its jump, δ, δ_1, δ_2, gradients have obtained nearly maximum values and the skin friction values have dropped significantly.

(vii) The gradients of δ, δ_1, increase are independent of $\mathrm{Re}_{\delta u}$ but the magnitude of these parameters value increase is much larger for lower $\mathrm{Re}_{\delta u}$.

(viii) The separation area displays strong 3-D effects. The asymmetry of the wall pattern increases with the $\mathrm{Re}_{\delta u}$ increase. Discussion of separation structures is presented in [19].

(ix) The normalized bifurcation point height decreases significantly with increasing $\mathrm{Re}_{\delta u}$. The only curved wall experimental point from literature [10] fits very well to the extrapolation of our curve. No comparison of the curve inclination could be made due to the insufficient amount of literature data. Our values are lower than that for flat walls, except for Seddon's result [2].

(x) The bifurcation topography indicates similarity. All our experimental points correlate on a single straight line. The point of Nebbeling [10] coincides with the correlation line, too.

References

[1] Ackeret, J., Feldmann, F., Rott, H.: Untersuchungen an Verdichtungsstößen und Grenzschichten in schnell bewegten Gasen. Bericht No. 10 des Instituts für Aerodynamik, ETH Zürich (1946).

[2] Seddon, J.: The flow produced by interactions of a turbulent boundary layer with a normal shock wave of strength sufficient to cause separation. ARC R and M 3502 (1967).

[3] Kooi, J. W.: Influence of free-stream Mach number on transonic shock-wave boundary-layer interaction. NRL MP 78012U.

[4] Padova, C., Falk, T. J.: Transonic shock wave-boundary layer interactions. AFOSR-TR-80-0694 (1980).

[5] Padova, C., Falk, T. J., Wittliff, C. E.: Experimental investigation of similitude parameters governing transonic shock-boundary layer interactions. AIAA Paper 80-0158 (1980).

[6] Vidal, R. J., Wittliff, C. E., Catlin, P. A., Sheen, B. H.: Reynolds number effects on the shock wave-turbulent boundary layer interaction at transonic speeds. AIAA Paper No. 73-661 (1973).

[7] Delery, J. M.: Experimental investigation of turbulence properties in transonic shock/boundary-layer interactions. AIAA J. **21**, 2, 180—185 (1983).

[8] Abbis, J. B., East, L. F., et al.: A study of the interaction of a normal shock wave and a turbulent boundary layer using a Laser anemometer. REA-TR-75141 (1976).

[9] Doerffer, P.: An experimental stand and measurement methodes to be used in turbulent boundary layer-normal shock wave interaction on a curved wall. Strömungsmechanik und Strömungsmaschinen 35/85, Universität Karlsruhe (1985).

[10] Nebbeling, C.: An experimental investigation of the interaction between a shock wave and a turbulent boundary layer on a convex wall. Report LR-**428** (May 1984), Delft University of Technology, Department of Aerospace Engineering.

[11] Doerffer, P.: The compression zone topography in the normal shock wave-turbulent boundary layer interaction. Strömungsmechanik und Strömungsmaschinen 38/66, Universität Karlsruhe (1986).

[12] Doerffer, P.: Boundary layer pressure distribution measurements in a transonic wind tunnel. Strömungsmechanik und Strömungsmaschinen 35/85, Universität Karlsruhe (1985).

[13] Myring, D. F.: The effects of normal pressure gradients on the boundary layer momentum integral equation. RAE Report 68214, August (1968).

[14] Om, D., Viegas, J. R., Childs, M. E.: Transonic shock-wave/turbulent boundary-layer interactions in a circular duct. AIAA J. **23**, 5, 707—714 (1985).

[15] Dallmann, U.: Topological structures of three-dimensional flow separations. DFVLR, IB 221-81A07, Göttingen (1983).

[16] Mateer, G. G., Viegas, J. R.: Effect of Mach and Reynolds number on a normal shock-wave/turbulent boundary-layer interaction. AIAA Paper **79**-1502.

[17] Doerffer, P.: An experimental investigation of a normal shock wave and a turbulent boundary layer interaction at a curved wall for: $M_w = 1.47$, $\mathrm{Re}_{\delta u} = 1.53 \cdot 10^5$. Strömungsmechanik und Strömungsmaschinen 38/86, Universität Karlsruhe (1986).

[18] Mateer, G. G., Brosh, A., Viegas, J. R.: A normal shock-wave turbulent boundary-layer interaction at transonic speeds. AIAA Paper **76**-161 (1976).

[19] Doerffer, P., Dallmann, U.: Separation structure produced by a normal shock wave/turbulent boundary layer interaction on a curved wall in a narrow wind tunnel. AIAA Conference, June 8—10, 1987, Honolulu, paper No. 87-1370.

[20] Bohning, R., Zierep, J.: Normal shock turbulent boundary layer interaction at a curved wall. AGARD CP No. **291**, Computations of Viscous-Inviscid Interactions, 17.1—17.8 1980.

[21] Koren, B., Bannink, W. J.: Numerical solution of transonic normal shock wave-boundary layer interaction using the Bohning-Zierep Model. Report LR-416, Delft University of Technology, January 1984.

[22] Om, D., Childes, M. E., Viegas, J. R.: An experimental investigation and a numerical prediction of a transonic normal shock wave/turbulent boundary layer interaction. AIAA Paper 82-0990, June 1982.

[23] Oswatitsch, K., Zierep, J.: Das Problem des senkrechten Stoßes an einer gekrümmten Wand. ZAMM **40**, T143 (1960) (Tagungsheft).

[24] Viegas, J. R., Horstman, C. C.: Comparison of multiequation turbulence models for several shock boundary layer interaction flows. AIAA J. **17**, 8, 811—820 1979.

P. Doerffer
Instytut Maszyn Przepływowych PAN
Gdańsk
Poland

J. Zierep
Institut für Strömungslehre
und Strömungsmaschinen
Universität Karlsruhe (TH)
Kaiserstrasse 12
D-7500 Karlsruhe
Federal Republic of Germany